Comparison of Proxy and Multi-Model Ensemble Means on Volcanic Aerosols' Hydrological Effects in Asian Monsoon and Westerlies-dominated Subregions

Zhihong Zhuo[1], Chaochao Gao[2], Ingo Kirchner[3], and Ulrich Cubasch[4]

[1]Institute of Meteorology, Freie Universität Berlin
[2]Zhejiang University
[3]Free University of Berlin
[4]Freie Universitaet Berlin

November 21, 2022

Abstract

Proxy-model comparisons show large discrepancies on volcanic aerosols' hydrological effects in the Asian monsoon region (AMR). This was mostly imputed to uncertainties of the single model used in previous studies. Here, we compared two groups of CMIP5 multi-model ensemble mean (MMEM) with the tree-ring-based reconstruction Monsoon Asia Drought Atlas (MADA PDSI), to examine their reliability on reflecting hydrological effects of the volcanic eruptions in 1300-1850 CE. Time series plots indicate that MADA PDSI and MMEMs agree on the significant drying effects of volcanic perturbation over the monsoon-dominated subregion, while mismatches exist over the westerlies-dominated subregion. Comparisons on spatial patterns suggest that MADA PDSI and MMEMs agree better in one year after the volcanic eruption than in the eruption year, and in subregions with more available tree ring chronologies. MADA PDSI and CMIP5 MMEMs agree on the drying effect of volcanic eruptions in western-East Asia, South Asian summer monsoon and northern East Asian summer monsoon (EASM). Model results suggest significant wetting effect in southern EASM and western-South Asia, which agrees with the observed hydrological responses to 1991 Mount Pinatubo eruption. Analysis on LME model simulations show similar hydrological responses. These results suggest that CMIP5 MMEM is able to reproduce volcanic eruptions' hydrological effects in southern AMR.

Comparison of Proxy and Multi-Model Ensemble Means on Volcanic Aerosols' Hydrological Effects in Asian Monsoon and Westerlies-dominated Subregions

Z. Zhuo[1], C.C. Gao[2], I. Kirchner[1] and U. Cubasch[1]

[1]Institute of meteorology, Freie Universität Berlin, Berlin, Germany.

[2]Department of Environmental Science, Zhejiang University, Hangzhou, China.

Corresponding author: Zhihong Zhuo (zhihong.zhuo@met.fu-berlin.de)

Key Points:

- Proxy and multi-model ensemble means agree/disagree on post-volcanic hydro-responses over the Asian monsoon/westerlies-dominated subregions
- Better agreement of spatial hydrological patterns is suggested in one year after the eruption and in subregions with more tree ring data
- Multi model ensemble means can reproduce the hydrological response to volcanic perturbations in southern Asian monsoon region

Abstract

Proxy-model comparisons show large discrepancies on volcanic aerosols' hydrological effects in the Asian monsoon region (AMR). This was mostly imputed to uncertainties of the single model used in previous studies. Here, we compared two groups of CMIP5 multi-model ensemble mean (MMEM) with the tree-ring-based reconstruction Monsoon Asia Drought Atlas (MADA PDSI), to examine their reliability on reflecting hydrological effects of the volcanic eruptions in 1300-1850 CE. Time series plots indicate that MADA PDSI and MMEMs agree on the significant drying effects of volcanic perturbation over the monsoon-dominated subregion, while mismatches exist over the westerlies-dominated subregion. Comparisons on spatial patterns suggest that MADA PDSI and MMEMs agree better in one year after the volcanic eruption than in the eruption year, and in subregions with more available tree ring chronologies. MADA PDSI and CMIP5 MMEMs agree on the drying effect of volcanic eruptions in western-East Asia, South Asian summer monsoon and northern East Asian summer monsoon (EASM). Model results suggest significant wetting effect in southern EASM and western-South Asia, which agrees with the observed hydrological responses to 1991 Mount Pinatubo eruption. Analysis on LME model simulations show similar hydrological responses. These results suggest that CMIP5 MMEM is able to reproduce volcanic eruptions' hydrological effects in southern AMR.

1 Introduction

Large explosive volcanic eruptions inject a large amount of sulfur into the stratosphere. After being converted to sulfate aerosols, they significantly cool the Earth's surface and warm the stratosphere by reflecting incoming solar radiation and absorbing both solar and longwave radiation (Robock 2000, 2015). Both observation and model results show that the direct surface cooling effects in summer (Kirchner et al., 1999) lead to significant summer precipitation reduction, especially in African and Asian monsoon regions (Trenberth & Dai, 2007; Iles et al., 2013; Iles & Hegerl, 2014; Zambri & Robock, 2016).

The Asian monsoon region (AMR, 8.75°S–56.25°N, 61.25°E–143.75°E, Cook et al., 2010) covers the most populated countries like China and India. The AMR has an uneven precipitation distribution due to different dominant winds, with much larger precipitation in the monsoon-dominated subregion (MDSR, southeast) than in the westerlies-dominated subregion (WDSR, northwest). Understanding the hydrological variation of volcanic perturbation in the AMR, is both biophysically and socioeconomically important (Dando, 2005). However, only limited studies aimed at this region, like Anchukaitis et al. (2010), Zhang et al. (2012), Man et al. (2014), Zhuo et al. (2014) and Stevenson et al. (2016, 2017), which investigated hydrological effects of historical volcanic eruptions in the past centuries. None of these studies took different dominated subregions into consideration in analysis. Their results show discrepancy even inversed spatial distribution of the hydrological effects between proxy reconstruction and single model simulation. The discrepancy was mostly imputed to model uncertainties due to a biased trust in proxy data. This can limit studies based on model simulations to understand potential mechanisms of volcanic aerosols' hydrological effects in this region. Proxy reconstructions also have uncertainty (PAGES 2k–PMIP3 group, 2015). PAGES Hydro2k Consortium (2017) suggests an equal view toward the uncertainties and limitations of proxy and models when comparing them with each other.

Recent studies report that an ensemble approach leads to a better estimation of climate change as it averages out unrelated model errors (Flato et al., 2013, Otto-Bliesner et al. 2016) and El Niño-Southern Oscillation (ENSO) effects (Iles et al., 2013, Stevenson et al. 2016). It even enhances climate prediction skills (Kadow et al. 2015), which are significantly affected by volcanic aerosols (Timmreck et al., 2016). Multi-model ensemble mean (MMEM) of the fifth phase of Coupled Model Intercomparison Project (CMIP5) shows a large improvement in reflecting global temperature and precipitation variation (Knutti & Sedlácek, 2012; Flato et al., 2013) as well as monsoon precipitation variation in East Asia (Song & Zhou, 2014; Kusunoki & Arakawa, 2015). Using MMEM of CMIP5 model output, responses of reduced temperature and summer monsoon rainfall to volcanic eruptions are also clearly detected in historical simulations (Zambri & Robock, 2016), and even in the “last millennium (LM)” experiment of CMIP5 (Zambri et al, 2017).

The climate effect to volcanic eruptions reported in Zambri et al. (2017) is more about the global scale. For future water management and coping strategy after volcanic perturbation, it’s important to concentrate on the regional scale. With consideration on different dominated subregions in the AMR, we compare proxy reconstruction and models in different subregions. This study tries to answer following questions: what are the similarities and discrepancies between proxy reconstruction and model on reflecting volcanic eruptions’ hydrological effects in different subregions of the AMR? Are CMIP5 MMEMs able to reproduce volcanic eruptions’ hydrological effects in the AMR? Following here are data and methods in section 2; comparisons of spatio-temporal hydrological patterns are presented in section 3; in section 4, we discuss the uncertainty source; we present our conclusions to answer the referred questions in section 5.

2 Data and Methods

2.1 Proxy Data and Covered Subregions

The proxy reconstruction data we adopt is Monsoon Asia Drought Atlas (MADA, Cook et al., 2010). It is a reconstruction of June-July-August (JJA) Palmer Drought Severity Index (PDSI) based on tree ring chronologies and PDSI reconstruction data (Dai et al., 2004), which has annual recordings from 1300 CE to 2005 CE and 2.5° × 2.5° spatial resolution in the AMR. Hereafter, I refer to MADA as MADA PDSI. The same as PDSI, positive MADA PDSI values represent wet conditions while negative values stand for dry conditions. Drought emerges when MADA PDSI falls below -0.5 while flood develops when it is over 0.5. It has been widely used as a reference data set for proxy-model comparisons on volcanic eruptions' hydrological effects in the AMR (Anchukaitis et al., 2010; Zhang et al., 2012; Wegmann et al., 2014, Stevenson et al., 2016, 2017).

In previous studies, proxy-model comparisons between MADA PDSI and models were conducted over the AMR (Anchukaitis et al., 2010; Wegmann et al., 2014; Stevenson et al., 2016, 2017). No selection was made regarding regional difference of dominant climate and data reliability. The AMR is not only dominated by monsoon climate, instead, different hydrological conditions are shown on two sides of the modern Asian summer monsoon limit (red dashed line in figure 1), to the northwest are the westerlies-dominated arid areas, whereas to the southeast are the monsoon-dominated humid areas (Dando, 2005; Herzschuh, 2006; Chen et al., 2008). It includes two monsoon subsystems - East Asian Summer Monsoon (EASM) and South Asian Summer Monsoon (SASM), which are usually separated by 100°E longitude (Herzschuh, 2006; Chiang et al., 2017). Considering this, we also performed time series analysis over the separated westerlies and monsoon-dominated subregions.

For spatial comparisons, as shown in figure 1, locations of the available tree ring chronologies (green dots) distribute irregularly over the AMR. This might cause different reliability of the MADA PDSI in different areas. According to Asian geographical distribution (Fan, 2017), the study area covers part of North Asia (NA), Central Asia (CA), and all the countries in East Asia (EA), South Asia (SA) and Southeast Asia (SeA). Considering the two monsoon systems, we separate the whole region into seven subregions (separated by purple boundary lines in figure 1) for more detailed discussion. We can see that western-East Asia (w-EA) is the subregion that has the most tree ring chronologies especially the ones dating back to 1300 CE (Cook et al., 2010). Among the monsoon-dominated subregions, SASM has more tree ring chronologies, followed by EASM and SeA. Among westerlies-dominated subregions, several tree ring chronologies are concentrated in the central part of North Asia (NA), most of them only date back to 1700 CE (Cook et al., 2010); western-South Asia (w-SA) and Central Asia (CA) have less tree ring sites.

Figure 1. The proxy reconstruction data MADA PDSI and the divided subregions. Modified from figure 1 of Cook et al. (2010). Red crosses show the 534 grid points. Green dots indicate the locations of the tree-ring chronologies. Seven subregions are divided by purple curves. Dashed red line indicates the modern Asian summer monsoon limit after Chen et al. (2008). Areas with yellow background indicate westerlies-dominated subregions: North Asia (NA), Central Asia (CA), western-South Asia (w-SA); areas with light green background indicate

monsoon-dominated subregions: East Asian summer monsoon (EASM, east of 100°E after Chiang et al. (2017)), South Asian summer monsoon (SASM) and Southeast Asia (SeA). Western-East Asia (w-EA) is the monsoon-westerlies transition zone.

2.2 Model ensembles and volcanic classifications

The "LM" experiment of CMIP5 was performed only by nine modelling groups performed the experiment (Schmidt et al., 2011). They can freely choose one of the two volcanic forcing data sets - GRA (Gao et al., 2008) and CEA (Crowley & Unterman, 2013). We separate models into two groups of MMEMs based on the adopted volcanic forcing data sets. To keep the same number of ensemble members involved in the MMEMs, we adopt six ensemble members of four models in each group, as shown in the green box in figure 2, more information about the model ensemble members are listed in table s1. Only GISS-E2-R model has three ensemble members, which might predominate the MMEM. Considering this, two set of MMEMs with four ensemble members (in black in the green box of figure 2), including only one ensemble member from GISS-E2-R, are tested. Two times of GRA volcanic forcing was used in the GISS-E2-R model simulations. This exaggerated volcanic forcing might cause excessive climate effects in the GRA-based group of CMIP5 MMEMs. To verify the model results, we also adopt all the available five ensemble members of the "volcanic only" experiment from the Last Millennium Ensemble (LME, Otto-Bliesner et al., 2016). This project performed large number of LM simulations with CESM1 (CAM5) model (Hurrell et al., 2013). In the "volcanic only" experiment, the GRA reconstruction (Gao et al., 2008) was adopted as the volcanic forcing dataset. Other forcing including solar variability, land use, GHGs and orbital changes were fixed to the same value as in 850 CE.

Figure 2. Volcanic years and northern hemisphere aerosol injection in GNH and CNH classifications. Red lines indicate that the volcanic events are included in both classifications. Model ensembles used in two classifications are shown in the green box, four model ensembles in black were used in the test of another round of multi-model ensemble means.

Following Zhuo et al. (2014), we construct two classifications - GNH and CNH - based on GRA and CEA volcanic forcing indices, with the chosen volcanic events that have larger northern hemisphere sulfate injection than 1991 Pinatubo eruption. The same as in Zhuo et al. (2014), for the events that without certain eruption date, we assume that they were erupted in spring; for the eruptions that occurred after August, we adjusted the eruption year to the next year, as their climatic impacts are likely to take effect during the next boreal summer. The chosen volcanic events and related aerosol injection magnitude are shown in figure 2, and the specific values are listed in table s2. MADA PDSI has recording in 1300-2005 CE, while CMIP5 "LM" experiment covers the period of 850-1849 CE. The overlapped period covering 1300-1849 CE were chosen as our core study period. In 1300-1849 CE, GNH classification has 12 volcanic events while CNH classification has 18 events. Different number of classified events may lead to different results between two classifications. We tested this uncertainty using classifications with nine events that are included in both classifications (as shown in red in figure 2). In order to verify the model results, analyses covering the whole period of 850-1849 CE are also made for CMIP5 PDSI and LME PDSI.

2.3 Methods

For better comparison between proxy reconstruction and models, CMIP5 “LM” experiment outputs are regridded to the same spatial resolution as MADA PDSI. Then, using the MATLAB program produced by Jacobi et al. (2013), model precipitation and temperature data, together with latitude and water-holding capacities (Webb et al., 2000), are transferred into PDSI. Finally, the MMEM of PDSI is calculated. Hereafter, it’s referred to as CMIP5 PDSI. Model ensemble members from LME have the same resolution. These model outputs are directly transferred into PDSI, and the multi-member mean is referred to as LME PDSI in this study.

Considering that PDSI combines both temperature and precipitation, we also adopted another widely used hydrological drought index: 12-months of Standardized Precipitation Index (SPI12, Mckee et al., 1993), which transferred only from model precipitation data. It indicates evident low water supply, especially in streams, reservoirs, and groundwater levels. This indicates the societal impact of continuous meteorological drought. Negative and positive values indicate specific drought and wet conditions. It indicates mild drought once SPI12 falls below zero. The same as CMIP5 PDSI, MMEM of SPI12 from CMIP5 “LM” experiment is calculated and referred to as CMIP5 SPI12. MADA PDSI only reflects the hydrological condition of the boreal summer season. To keep model data the same as MADA PDSI, we analyze summer JJA mean of CMIP5 PDSI and CMIP5 SPI12 in this study.

After pretreatment of the classifications and hydrological data, we conduct Superposed Epoch Analysis (SEA, Haurwitz & Brier, 1981) on hydrological indices (MADA PDSI, CMIP5 PDSI, CMIP5 SPI12 and LME PDSI) for 11 years (-5 to 5) surrounding the eruption year (year 0) in each classification. To study the significance of the hydrological effects, we conduct Monte Carlo model tests (Adams et al., 2003) based on the null hypothesis that there is no relationship between volcanoes and hydrological conditions. Each volcanic event is randomly reassigned a new eruption year in the study period, and then the average values of the hydrological indices are calculated for the 11 years. For significance tests of time series analysis, 10000 times of resampling are made on regional averaged hydrological indices. For spatial analyses, 1000 times of resampling are made on each grid. This builds a random distribution, against which our SEA results are considered to be statistically significant at the 95% (99%) confidence level when they exceed the 95% (99%) range of the Monte Carlo results. To quantify the same drought and wet areas between proxy and MMEMs, we counted the number of grid cells that have same sign between MADA PDSI and CMIP5 PDSI/SPI12, then calculated their percentage in each subregion.

3 Comparison of spatio-temporal hydrological patterns

3.1 Temporal hydrological responses to volcanic classifications

Figure 3 shows the SEA results of MADA PDSI, CMIP5 PDSI and CMIP5 SPI12 over the Asian monsoon region for GNH and CNH volcanic classifications. As shown in figure 3a, MADA PDSI decreases in one year after the eruption (year 1), and significant drying effect emerges in two and three years after the eruption (year 2 and year 3). CMIP5 PDSI decreases promptly and sharply in the eruption year (year 0). The significant drying effects last for three years, and gradually recover to normal condition in year 4. Similarly, CMIP5 SPI12 decreases rapidly in year 0 and year 1, after the strongest drying effects in year 1, it gradually recovers in year 2 and turns to normal condition in year 3. This indicates an agreement between MADA PDSI and CMIP5 PDSI/SPI12 on the drying effects of the volcanic eruptions, although with one year of time lag in MADA PDSI compared to CMIP5 PDSI/SPI12, and the magnitude shown in CMIP5 PDSI/SPI12 are much larger than that in MADA PDSI. This is probably due to exaggerated two times of the GRA forcing used in the GISS-E2-R model simulations. Figure 3b shows hydrological responses to the CNH volcanic eruptions. The response tendency is similar to that in the GNH classification, MADA PDSI increases before the eruption, and decreases in year 1 and year 2; CMIP5 PDSI and CMIP5 SPI12 decreases promptly in year 0 and reach the lowest value in year 1, then gradually recovers from year 2. Comparing to the significant results (even at the 99% confidence level) in the GNH classification, the results are less significant in the CNH classification, but the magnitudes between MADA PDSI and CMIP5 PDSI/SPI12 are closer to each other. The different scale between MMEMs of two classifications might also result from different number of superposed volcanic events. But differences still exist when the classifications are constructed only with the same nine events in both volcanic forcing indices (shown in red in figure 2). Crowley et al. (2013) suggested that volcanic forcing in the GRA index is overestimated. When reconstructing the CEA index, they used a scaling of two-thirds to calculate the forcing of the explosive eruptions which are larger than 1991 Pinatubo eruption. Volcanic events included in the CNH classification are affected by this scaling process, which result in the minor hydrological responses.

Figure 3. Temporal SEA results of MADA PDSI (blue lines), JJA mean CMIP5 PDSI (red lines) and CMIP5 SPI12 (pink lines) corresponding to GNH (a) and CNH (b) volcanic classifications in 1300-1850 CE over the Asian monsoon region. The thinner lines stand for the relative Monte Carlo model results at the 95% confidence level. The asterisks represent the year that passed the Monte Carlo model tests at the 99% confidence level. Year 0 represents the identified eruption year by volcanic forcing indices, negative and positive years represent relative years before and after the eruption.

Figure 4: Same as figure 3 but for LME PDSI in 1300-1849 CE, and both LME PDSI and CMIP5 PDSI in 850-1849 CE.

The exaggerated two times-GRA forcing used in the GISS-E2-R model simulations also cause the excessive climate response in the GNH classification. As shown in figure 4, temporal SEA results of LME PDSI over two periods show significant drying effects in year 0 and the significant drying effects last to year 1. CMIP5 PDSI shows excessive drying effects over the whole period, which is similar to that shown in figure 3a over the core study period. This confirms the findings shown in Zhuo et al. (2014) that larger volcanic aerosol magnitude leads to larger drying effect. The significant drying effects in two to three years after the volcanic eruptions agree with previous research findings (Anchukaitis et al., 2010; Man et al., 2014; Zhuo et al., 2014; Liu et al, 2016), which is prominent in the general background of a significant reduction in global precipitation (Iles & Hegerl, 2014).

Temporal SEA analysis over the whole region confound the different climate conditions in the westerlies and monsoon-dominated subregions. Additionally, temporal SEA results over the separated westerlies and monsoon-dominated subregions are presented. Figure 5a shows different hydrological responses in the WDSR, as MADA PDSI in both the GNH (solid blue line) and CNH (dotted blue line) classifications increase from the negative in year -3 to the positive in year -2. The wet conditions extend to in year 0 to year 2, then turn to dry conditions in year 3 to year 5. MADA PDSI in year 1 and year 2 in the CNH classification pass the significance test, but only at the 95% confidence level, and the values do not exceed the largest value in year -5 and the smallest value in year 5. This might indicate that the hydrological response to volcanic perturbations in the WDSR is insensitive to volcanic forcing. However, CMIP5 PDSI and CMIP5 SPI12 in the GNH classification show highly significant drying effects in year 0 to year 3 at the 99% confidence level. In the CNH classification, CMIP5 SPI12 shows significant drying effects in year 1 and year 2, but CMIP5 PDSI does not indicate drying effect, instead only significant wetting variation are shown in year -1. This indicates a large difference between MADA PDSI and CMIP5 PDSI/SPI12 in the WDSR. Considering the exaggerated volcanic forcing used in the GNH classification, this might suggest that the wetting or drying effect in this insensitive area depends largely on the magnitude of the injected volcanic aerosols. In the MDSR (figure 5b), MADA PDSI and CMIP5 PDSI/SPI12 in two classifications all agree on the drying effects in year 0 and year 1, and the recovering from year 2 onwards. We note that the time-lag effect of proxy data probably exists. As MADA PDSI decreases in year 0, but the significant drying effects are shown in year 1, whereas, CMIP5 PDSI/SPI12 show a sharp decrease in year 0 and the significant drying effects extend to year 1.

Figure 5: Temporal SEA results of MADA PDSI (blue lines), JJA mean CMIP5 PDSI (red lines) and CMIP5 SPI12 (pink lines) corresponding to GNH (solid lines) and CNH (dashed lines) volcanic classifications in 1300-1850 CE over the westerlies-dominated subregion (a) and monsoon-dominated subregion (b). Small and large circle dots indicate the years are significant at the 95% and 99% confidence level.

Figure 6 shows the temporal SEA results of LME PDSI over both periods and CMIP5 PDSI over the whole period over the separated westerlies and monsoon-dominated subregions. In the WDSR, CMIP5 PDSI indicates significant drying effects over the whole period (850-1849). LME PDSI increases in year 1 and decreases from year 2 to year 5 over both periods. This is similar to the response tendency of MADA PDSI in the GNH classification (figure 5a), but both results did not pass the significance tests even at the 95% confidence level. In the MDSR, model results all suggest consistent drying effects in the year 0 and year 1, and then gradually recover in year 2.

Figure 6: Same as figure 5 but for LME PDSI in 1300-1849 CE, and both LME PDSI and CMIP5 PDSI in 850-1849 CE.

3.2 Spatial patterns of the hydrological response

Considering uncertainties of spatial responses arising from the estimated aerosol magnitude in volcanic forcing reconstructions, following discussions focus on horizontal distribution of the hydrological tendencies. To quantify the similarity of drought and wet areas between proxy and model, in figure 7, we show percentages of grid cells that have same sign between MADA PDSI and CMIP5 PDSI/SPI12 in different subregions in year 0 (in magenta) and year 1 (in red). When separated into two dominated subregions, it is hard to find out consistent variation tendency, except that the percentage increases from year 0 to year 1 in the WDSR while decreases in the MDSR, and different ensemble members show larger difference in the WDSR than in the MDSR.

When separated into seven subregions with consideration of the spatial coverage of tree ring chronologies, the percentages show large differences in different subregions. Four subfigures all indicate that the largest similarity between MADA PDSI and CMIP5 PDSI/SPI12 emerges in the w-EA, where the most tree ring chronologies are available, in both year 0 and year 1. It also shows fewest difference among different ensemble members. Single model and MADA PDSI have large uncertainty. The consistency among different groups and ensemble members improve the reliability of reflecting the hydrological effects of volcanic eruptions by both proxy and models. Better agreements are then shown in SASM and EASM, with less difference among different ensemble members than in w-SA and SeA. These results suggest that proxy and models agree better in the subregions with more tree ring chronologies, which indicates an important role the available tree ring chronology plays on the reliability of proxy reconstruction data. The percentages are mainly larger in year 1 than in year 0, except for NA and CA, where have the fewest tree ring chronologies. This is consistent with the temporal SEA results, and spatially quantify that MADA PDSI and CMIP5 MMEMs agree better in monsoon-dominated subregions in year 1.

Figure 7: Histogram on percentages of grid cells that have same sign between MADA PDSI and CMIP5 PDSI/SPI12 in the GNH classification (a/b) and CNH classification (c/d). Columns indicate the percentages in the westerlies-dominated subregion (WDSR) and monsoon-dominated subregion (MDSR) as well as in the seven subregions in year 0 (in magenta) and year 1 (in red). Different marks indicate the percentages between MADA PDSI and PDSI/SPI12 of different single ensemble members.

Figure 8: Spatial response of MADA PDSI (a), JJA mean CMIP5 PDSI (b) and CMIP5 SPI12 (c) to GNH volcanic classification in 1300-1850 CE in the Asian monsoon region. The grid cells marked by black dots and slashes denote areas that passed the Monte Carlo model significance tests at the 95% and 99% confidence levels. Year 0 represents the volcanic eruption year by volcanic forcing indices, negative and positive years represent relative years before and after the eruption.

To investigate the spatial distribution of the hydrological variation, we show the spatial patterns of the superposed hydrological responses to the GNH classification in figure 8. CMIP5 PDSI (figure 8b) shows drier conditions before the eruption (Year -5 to -1 ave) than that in MADA PDSI (figure 8a), but with a similar southeast-wet-northwest-dry dipolar distribution. MADA PDSI shows wet conditions in NA, northeast EASM and SeA in year 0 and in CA in year 1. However, most results do not pass the significance test. Significant drying effects develop in w-EA in year 0 and extends to SASM and northern EASM in year 1; the drying effects are reflected by the disappearance of the wet areas in SeA. Consistent with the temporal SEA results, MADA PDSI shows the strongest effect in year 1, with drying effects in monsoon-dominated subregions and wetting effects in westerlies-dominated subregions. This gradually reverses in year 2 and turns to wet in the monsoon-dominated subregions while drought in the westerlies-dominated subregions in year 3. Comparing to MADA PDSI, CMIP5 PDSI shows faster and longer effects, with overall significant drying effects in year 0 to year 2 at the 99% confidence level, except for the wet areas in w-SA and southern EASM. Similarly, drought areas in the monsoon-dominated subregions turn to wet in year 3, while drying effects maintain in the westerlies-dominated subregions (figure 8b). These patterns are well verified by CMIP5 SPI12, which displays similar patterns in figure 8c. From the hydrological variation tendency, proxy-model comparisons suggest similar drying to wetting variation in monsoon-dominated subregions (EASM, SASM and SeA), with faster and longer effects shown in the models than in the proxy data. This might result from the excessive volcanic forcing used in the GISS-E2-R model simulations. The ecological time lag-effect of the tree-ring based proxy reconstruction (Wu et al., 2005) and the dating uncertainty of volcanic eruption might also contribute to the difference. General agreements are shown in w-EA, where has a dense coverage of tree ring chronologies. In the westerlies-dominated subregions with rare tree rings, MADA PDSI shows wetting to drying transitions, CMIP5 PDSI/SPI12 show continuous drying effects in CA and NA, but wetting effects in w-SA. This is consistent with the temporal SEA results shown in figure 5, that MADA PDSI and CMIP5 PDSI/SPI12 agree on the tendency of the hydrological response to volcanic perturbation in the MDSR, while discrepancies exist in the WDSR.

In the CNH classification (figure 9), MADA PDSI (figure 9a) and CMIP5 PDSI (figure 9b) indicate weaker effects of volcanic perturbations. It shows similar hydrological patterns as that in the GNH classification (figure 8a and 8b), except that CMIP5 PDSI shows limited response in CA and NA (figure 9b). The drying effects shown in the GNH classification (figure 8 (b)) might be caused by the response to the exaggerated volcanic forcing used in GISS-E2-R model simulations. CMIP5 SPI12 (figure 9c) indicates even weaker effects, but the obvious drought areas agree well with those CMIP5 PDSI patterns. Better agreement between MADA PDSI and CMIP5 PDSI/SPI12 occurs in the subregions with more available tree ring chronologies. Highly significant results of CMIP5 PDSI/SPI12 in the GNH and CNH classifications indicate the consistency of MMEMs on reproducing volcanic aerosols' hydrological effects in southern AMR. In CA and NA, discrepancies between MADA PDSI and CMIP5 PDSI/SPI12 do not allow drawing definite conclusions.

To verify model results, we show spatial patterns of LME PDSI over both periods (1300-1849 and 850-1849) and CMIP5 PDSI over the whole period (850-1849) in figure 10, CMIP5 PDSI shows similar patterns even when extending the period to the whole 1000 years (figure 10c). Similar patterns are also shown in LME PDSI over both periods, especially in southern Asian monsoon region. The drought and wet areas are not totally same among these different model results. However, with different model resolutions, it is fastidious to have complete matches. This indicates that the study periods, the number of the superposed events and the aerosol magnitude do not affect much the spatial patterns of the hydrological effects. These similar patterns support the reliability of models on reproducing the hydrological effects of volcanic eruptions in southern Asian monsoon region. LME PDSI also suggest slight drying effect in NA from year 0 to year 2 over both periods. These PDSI patterns might suggest that drying effects can emerge in NA and CA with strong enough volcanic forcing.

Figure 9: Same as figure 8 but response to CNH volcanic classification.

Summarizing the proxy-model comparison on the spatio-temporal patterns of hydrological responses to volcanic eruptions, one finds similar drying effects in the MDSR while discrepancies exist in the WDSR. Results show a better agreement on the spatial patterns in w-EA, SASM and EASM where there are more available tree ring chronologies. This poses an advance on previous studies. Anchukaitis et al. (2010) showed an east-dry-west-wet dipolar pattern by single model CSM1.4. Zhang et al. (2012) showed wetting effects in central Asia by ensemble mean of single model MPI-COSMOS. MADA PDSI shows different spatial pattern

(Anchukaitis et al., 2010; Zhang et al., 2012). Stevenson et al. (2016, 2017) also showed different patterns between MADA PDSI and ensemble mean of single model CESM. These spatial comparisons were made only in the eruption year. In comparison, our results were based on MMEMs and showed significant improvements. Spatial comparisons of three years are presented and suggest a better agreement in year 1 than in year 0. CMIP5 PDSI and CMIP5 SPI12 verify each other between two classifications with highly significant results. Similar spatial patterns of LEM PDSI indicate the reliability of model simulations. They agree better in the monsoon-dominated subregions with MADA PDSI responding to volcanic eruptions. In the southern Asian monsoon region, spatial patterns of MMEMs in year 0 and year 1 agree well with precipitation anomaly pattern after Krakatau and Pinatubo eruptions shown in Zambri and Robock (2016). The identified wet areas in EASM are close to that in Gao and Gao (2018), which showed an increased precipitation over the Yangtze-Huaihe River valley using Feng et al. (2013) precipitation reconstruction. The patterns are also consistent with the observed precipitation and PDSI variations shown in Trenberth and Dai (2007), with a drying effect in SASM, SeA and northern EASM, and wetting effect in w-SA and southern EASM after the Mount Pinatubo eruption. In the northern Asian monsoon region, except for PDSI, which suggest drying effects (Trenberth and Dai, 2007), limited effects are shown in precipitation (Trenberth and Dai, 2007; Zambri and Robock, 2016) and runoff variations (Trenberth and Dai, 2007). These results indicate the reliability of MMEMs in reflecting the spatio-temporal patterns of hydrological response to volcanic perturbations in the Asian monsoon region, except for Central Asia and North Asia; one cannot draw definite conclusion in these two subregions, because CMIP5 PDSI and CMIP5 SPI12 in the CNH classification display no impact, and there are limited available observations in these subregions to validate the results.

Figure 10: Same as figure 8 but for LME PDSI in 1300-1849 CE, and both LME PDSI and CMIP5 PDSI in 850-1849 CE.

4 Discussion on uncertainty source

Results suggest large discrepancy between MADA PDSI and models in the westerlies-dominated subregions with fewer available tree ring chronologies. It suggests a better agreement in one year after the eruption instead of in the eruption year. These discrepancies indicate the uncertainty of the results deriving from the data source and analysis process. As suggested by PAGES Hydro2k Consortium (2017), we treat proxy reconstruction and model data equally, and discuss uncertainties and limitations of both MADA PDSI and CMIP5 PDSI/SPI12. From the temporal SEA results of the Asian monsoon region (figure 3), we can see that CMIP5 PDSI/SPI12 agrees with MADA PDSI on the drying effects of explosive volcanic eruptions. CMIP5 PDSI shows stronger effects than MADA PDSI in the GNH classification. Stronger effects are also shown in the GNH classification than that in the CNH classification. This is caused by both the exaggerated volcanic forcing used in the GISS-E2-R model ensemble members and the reduced amplitude of the forcing in the CEA reconstruction (Crowley et al., 2008, 2013). This can be verified by the results of LME PDSI. Besides, faster responses are shown in CMIP5 PDSI/SPI12 than that in MADA PDSI in both classifications. This reflects the time lag effect in the tree-ring-based ecological response compared to the meteorological response in the model simulation (Wu et al., 2005).

Volcanic years identified in volcanic forcing indices deviate from the reality. Superposed volcanic classification averages out the effect of single event, but the dating uncertainty of volcanic events can cause large uncertainty on the hydrological effects reflected by MADA PDSI. Uncertainty of eruption month coming from the volcanic forcing indices also bring uncertainty on defining the eruption year. This might explain the abnormal wetting effect in year 0 shown by MADA PDSI (figure 3), which was also identified in Anchukaitis et al. (2010) after different superposed volcanic events. To investigate these uncertainties, we test several different classifications. Volcanic years and the number of included events in different classifications are listed in table s3. We show response of MADA PDSI to these different classifications in figure 11. The same as in the GNH and CNH classifications, MADA PDSI suggests wetting effects in year 0 in the GCNH classification. However, MADA PDSI starts to decrease in year 0, and drops to the lowest value in year 2 and year 3 in SNH and A07 classifications, respectively. SNH classification is based on the most start-of-the-art volcanic forcing reconstruction, which largely improved the dating accuracy (Sigl et al., 2015), while A07 classification includes only those five explosive eruptions that are the most well-known events during the past centuries. These two classifications have minimum dating uncertainty among the volcanic classifications used in this study. This indicates that the dating uncertainty largely affect the climate response especially in year 0. The wetting effects shown by MADA PDSI are probably result from dating uncertainty of the volcanic events.

Figure 11: Temporal SEA results of MADA PDSI corresponding to different classifications of volcanic eruptions.

The temporal SEA results of two separated subregions (figure 5) suggest an agreement between MADA PDSI and CMIP5 PDSI/SPI12 in the MDSR while large discrepancies exist in the WDSR. Quantification of the grid cells with same sign between MADA PDSI and CMIP5 PDSI/SPI12 indicates a better agreement in subregions with more tree ring chronologies and in the second summer after the volcanic perturbations. This might explain partly the spatial proxy-model discrepancies suggested by precious studies (Anchukaitis et al., 2010; Zhang et al., 2012; Stevenson et al., 2016, 2017), because comparisons were only made in the first summer after the eruptions. Comparisons on spatial patterns of the hydrological effects show large discrepancies in westerlies-dominated subregions with limited tree ring chronologies. This reveals the limitation of MADA PDSI caused by the spatial coverage of tree ring chronologies. The drying tendencies in NA and CA reflected by CMIP5 PDSI/SPI12 in the GNH classification might be realistic, but it might be misleading patterns coming from the exaggerated volcanic forcing used in the GISS-E2-R model ensemble members. This exaggerated forcing also contributes to the faster and longer drying effects of volcanic perturbation in monsoon-dominated subregions.

Spatial SEA results (figure 8) indicate significant wetting effects in NA by MADA PDSI, which are opposite to the drying effects shown by CMIP5 PDSI and LME PDSI in the GNH classification. Similar discrepancies were also presented in Liu et al. (2016). This may indicate data uncertainties of MADA PDSI, especially in westerlies-dominated subregions where are short of tree ring chronologies that go back to 1300 CE (Cook et al., 2010). However, we would like to point out that the models also suggest wetting effects in the western areas, and the wet areas vary a bit in different groups of model ensemble means, which have different forcing magnitudes. Thus, the discrepancies can be also caused by the uncertain aerosol magnitudes and the consequent uncertain effects shown in the models. The difference in resolution of both proxy reconstruction and models also introduces uncertainties.

A limited number of ensemble members might bring uncertainty to the model results. Especially, three ensemble members of GISS-E2-R model might have a predominant effect on the MMEMs. However, when testing MMEMs with only four members (members in black in figure 2), which include only one member of GISS-E2-R model, temporal and spatial patterns remain largely unchanged. Deviation of the model-based analysis between two classifications can come from the number of classified events based on volcanic forcing indices. When testing the classifications with the same nine events in both indices (marked in red in figure 2), temporal and spatial patterns remain largely constant.

The internal variability of the climate system often brings uncertainty on detecting the hydrological effects of volcanic eruptions, especially the hardly constrained effects of the concurrent ENSO events (Adams et al., 2003; Li et al., 2013; khodri et al., 2017; Stevenson et al., 2016, 2017). The effect of eruption seasons on the circulation and ENSO can bring extra uncertainties (Stevenson et al., 2017). All these might contribute to the proxy-model discrepancies, especially in the initial phase and the phase-out period of the hydrological effects. Following the method in Iles et al. (2013), we test this uncertainty through repeating the SEA analysis after regressing out the effect of ENSO. Consistent with Iles et al. (2013) and Iles and Hegerl (2014), it only results in a lower response in amplitude, but the temporal and spatial patterns remain largely unchanged. In addition, previous researches show that volcanic eruptions can affect the hydrological condition through affecting the evolution of ENSO in time, but with large contradictory findings (Adams et al., 2003; Li et al., 2013; Stevenson et al., 2016; Wang et al., 2017; Liu et al., 2018; Sun et al., 2018). This is an additional source contributing to proxy-model discrepancies. Future improvement of volcanic forcing reconstructions, model simulations, proxy reconstructions and observations will lead to a better understanding and reconciling the proxy-model discrepancies.

5 Conclusions

Previous studies show large discrepancies between proxy and model on volcanic aerosols' hydrological response patterns in the Asian monsoon region. In this study, we use tree ring-based proxy data MADA PDSI and a number of model ensemble members from CMIP5 and LME, to compare their spatio-temporal hydrological response to two classified volcanic events in 1300 – 1850 CE in subregions of monsoon Asia.

Our temporal SEA results show that MADA PDSI and models agree on the significant drying effects of volcanic aerosols in the MDSR, while disagreement exists in the WDSR. Spatial comparisons indicate better agreement in subregions with more available tree ring chronologies. Especially in w-EA, where has the most available tree ring chronologies dating back to 1300 or even earlier, MADA PDSI agrees with models on the significant drying effects of volcanic aerosols. In monsoon-dominated subregions, MADA PDSI and models show similar drying to wetting variations after the volcanic perturbations, with rapider and prolonged drying effects shown by models, which might result from the overestimated aerosol magnitude in the volcanic forcing index and the time-lag effect of tree ring-based proxy reconstruction data. The effect of uncertain eruption season on the circulation and the definition of the eruption year might also contribute to their difference. Because of these uncertainties, MADA PDSI and models show better consistency in year 1, with significant drying effects in northern EASM, SASM and SeA, and opposite wetting effects in southern EASM. In westerlies-dominated subregions, where lack of tree ring chronologies, MADA PDSI and models show larger discrepancies. Since two groups of CMIP5 MMEMs and LME PDSI all shows similar patterns, and with verification from previous studies, we propose the reliability of CMIP5 MMEMs on reflecting the wetting effects in w-SA. In CA and NA subregions, MADA PDSI shows significant wetting effects. CMIP5 MMEMs in GNH show significant drying effects, LME PDSI shows some drying effects only in NA, whereas CMIP5 MMEMs in CNH show limited response. Considering the lack of cross-verification, we do not draw certain conclusion in these two subregions.

Through spatio-temporal comparisons, we exam the reliability of MADA PDSI and CMIP5 MMEMs on reflecting the patterns of hydrological responses to volcanic perturbations. It suggests larger reliability of MADA PDSI in subregions with more available tree ring chronologies. Comparisons between proxy, observation and models indicate that CMIP5 MMEMs are reliable to reflect the hydrological effects of volcanic aerosols in southern Asian monsoon region. Further analysis on CMIP6 and improved proxy reconstruction data will contribute to verify these results better.

This study discusses the long-standing proxy-model discrepancy problem. We treat the uncertainties and limitations of both proxy and models equally. This contributes to better interpretations on the results, and shed new light on the reliability of both proxy data and CMIP5 model simulations on reflecting the hydrological effects of historical volcanic eruptions in Asian subregions. This might promote further researches like mechanism exploration that based highly on model simulations, which is important for better evaluating effects of both historical and future volcanic eruptions and feasibility of future choices on stratospheric aerosol injection engineering.

Acknowledgments

This work is supported by China Scholarship Council (CSC). The authors acknowledge the climate modelling groups listed in figure 1 and the Last Millennium Ensemble project group for producing and making their model outputs available, and the German Climate Computing Center (DKRZ, https://www.dkrz.de/) for making the CMIP5 model output and the computational resources available. CMIP5 model outputs are downloaded from https://esgf-data.dkrz.de/search/cmip5-dkrz/. LME model outputs are downloaded from https://www.earthsystemgrid.org/dataset/ucar.cgd.ccsm4.CESM_CAM5_LME.atm.proc.monthly_ave.html. We thank Kirstin Krüger and Claudia Timmreck for helpful discussions.

References

Adams, J. B., Mann, M. E., & Ammann, C. M. (2003). Proxy evidence for an El Niño-like response to volcanic forcing. *Nature, 426*(6964), 274-278. doi:10.1038/nature02101

Anchukaitis, K. J., Buckley, B. M., Cook, E. R., Cook, B. I., D'Arrigo, R. D., & Ammann, C. M. (2010). Influence of volcanic eruptions on the climate of the Asian monsoon region. *Geophysical Research Letters, 37*(22), L22703. doi:10.1029/2010gl044843

Chen, F., Yu, Z., Yang, M., Ito, E., Wang, S., Madsen, D. B., et al. (2008). Holocene moisture evolution in arid central Asia and its out-of-phase relationship with Asian monsoon history. *Quaternary Science Reviews, 27*(3-4), 351-364. doi:10.1016/j.quascirev.2007.10.017

Chiang, J. C. H., Swenson, L. M., & Kong, W. (2017). Role of seasonal transitions and the westerlies in the interannual variability of the East Asian summer monsoon precipitation. *Geophysical Research Letters, 44*(8), 3788-3795. doi:10.1002/2017gl072739

Cook, E. R., Anchukaitis, K. J., Buckley, B. M., D'Arrigo, R. D., Jacoby, G. C., & Wright, W. E. (2010). Asian monsoon failure and megadrought during the last millennium. *Science, 328*(5977), 486-489. doi:10.1126/science.1185188

Crowley, T. J., & Unterman, M. B. (2013). Technical details concerning development of a 1200 yr proxy index for global volcanism. *Earth System Science Data, 5*(1), 187-197. doi:10.5194/essd-5-187-2013

Dai, A. G., Trenberth, K. E., & Qian, T. T. (2004). A global dataset of Palmer Drought Severity Index for 1870–2002: Relationship with soil moisture and effects of surface warming, *Journal of Hydrometeorology, 5*(6), 1117–1130.

Dando, W. A. (2005). Asia, climate of Siberia, Central and East Asia. *Encyclopedia of Earth Sciences Series*. Dordrecht: Springer. https://doi.org/10.1007/1-4020-3266-8_19

Dufresne, J. L., Foujols, M. A., Denvil, S., Caubel, A., Marti, O., Aumont, O., et al. (2013). Climate change projections using the IPSL-CM5 Earth System Model: from CMIP3 to CMIP5. *Climate Dynamics, 40*(9-10), 2123-2165. doi:10.1007/s00382-012-1636-1

Fan, J. (Ed.). (2017). *Geography in the second volume of seventh grade*. Beijing: People's Education.

Feng, S., Hu, Q., Wu, Q., & Mann, M. E. (2013). A Gridded Reconstruction of Warm Season Precipitation for Asia Spanning the Past Half Millennium. *Journal of Climate, 26*(7), 2192-2204. doi:10.1175/jcli-d-12-00099.1

Flato, G., J., Marotzke, B., Abiodun, P., Braconnot, S.C., Chou, W., Collins, P., et al. (2013). Evaluation of climate models. In Stocker, T.F., Qin, D., Plattner, G. K., Tignor, M., Allen, S.K., Boschung, J. et al. (Eds.), *Climate Change 2013: The Physical Science Basis. Contribution of Working Group I to the Fifth Assessment Report of the Intergovernmental Panel on Climate Change* (pp. 741-866), Cambridge: Cambridge University

Gao, C., & Gao, Y. (2018). Revisited Asian Monsoon Hydroclimate Response to Volcanic Eruptions. *Journal of Geophysical Research, 123*, 7883-7896. doi:10.1029/2017JD027907

Gao, C., Robock, A., & Ammann, C. (2008). Volcanic forcing of climate over the past 1500 years: An improved ice core-based index for climate models. *Journal of Geophysical Research, 113*(23), D23111. doi:10.1029/2008jd010239

Gent, P. R., Danabasoglu, G., Donner, L. J., Holland, M. M., Hunke, E. C., Jayne, S. R., et al.

(2011). The Community Climate System Model Version 4. *Journal of Climate, 24*(19), 4973-4991. doi:10.1175/2011jcli4083.1

Giorgetta, M. A., Jungclaus, J., Reick, C. H., Legutke, S., Bader, J., Böttinger, M., et al. (2013). Climate and carbon cycle changes from 1850 to 2100 in MPI-ESM simulations for the Coupled Model Intercomparison Project phase 5. *Journal of Advances in Modeling Earth Systems, 5*(3), 572-597. doi:10.1002/jame.20038

Haurwitz, M. W., & Brier, G. W. (1981). A critique of the superposed epoch analysis method - Its application to solar weather relations. *Monthly Weather Review, 109*(10), 2074–2079.

Herzschuh, U. (2006). Paleo-moisture evolution in monsoonal Central Asia during the last 50,000 years. *Quaternary Science Reviews, 25*(1-2), 163-178. doi:10.1016/j.quascirev.2005.02.006

Iles, C. E., & Hegerl, G. C. (2014). The global precipitation response to volcanic eruptions in the CMIP5 models. *Environmental Research Letters, 9*(10), 104012. doi:10.1088/1748-9326/9/10/104012

Iles, C. E., Hegerl, G. C., Schurer, A. P., & Zhang, X. (2013). The effect of volcanic eruptions on global precipitation. *Journal of Geophysical Research: Atmospheres, 118*(16), 8770-8786. doi:10.1002/jgrd.50678

Jacobi, J., Perrone, D., Duncan, L. L., & Hornberger, G. (2013). A tool for calculating the Palmer drought indices. *Water Resources Research, 49*(9), 6086-6089. doi:10.1002/wrcr.20342

Kadow, C., Illing, S., Kunst, O., Rust, H. W., Pohlmann, H., Müller, W. A., & Cubasch, U. (2015). Evaluation of forecasts by accuracy and spread in the MiKlip decadal climate prediction system. *Meteorologische Zeitschrift*. doi:10.1127/metz/2015/0639

Khodri, M., Izumo, T., Vialard, J., Janicot, S., Cassou, C., Lengaigne, M., et al. (2017). Tropical explosive volcanic eruptions can trigger El Nino by cooling tropical Africa. *Nature Communications, 8*(1), 778. doi:10.1038/s41467-017-00755-6

Kirchner, I., Stenchikov, G. L., Graf, H.-F., Robock, A., & Antuña, J. C. (1999). Climate model simulation of winter warming and summer cooling following the 1991 Mount Pinatubo volcanic eruption. *Journal of Geophysical Research: Atmospheres, 104*(D16), 19039-19055. doi:10.1029/1999jd900213

Knutti, R., & Sedláček, J. (2012). Robustness and uncertainties in the new CMIP5 climate model projections. *Nature Climate Change, 3*(4), 369-373. doi:10.1038/nclimate1716

Kusunoki, S., & Arakawa, O. (2015). Are CMIP5 models better than CMIP3 models in simulating precipitation over East Asia? *Journal of Climate, 28*(14), 5601-5621. doi:10.1175/jcli-d-14-00585.1

Li, J., Xie, S. P., Cook, E. R., Morales, M. S., Christie, D. A., Johnson, N. C., et al. (2013). El Niño modulations over the past seven centuries. *Nature Climate Change, 3*(9), 822-826. doi:10.1038/nclimate1936

Liu, F., Chai, J., Wang, B., Liu, J., Zhang, X., & Wang, Z. (2016). Global monsoon precipitation responses to large volcanic eruptions. *Sci Rep, 6*, 24331. doi:10.1038/srep24331

Liu, F., Li, J. B., Wang, B., Liu, J., Li, T., Huang, G., & Wang Z. Y. (2018). Divergent El Niño responses to volcanic eruptions at different latitudes over the past millennium. *Climate Dynamics, 50*(9-10), 3799-3812. https://doi.org/10.1007/s00382-017-3846-z

Man, W., Zhou, T., & Jungclaus, J. H. (2014). Effects of large volcanic eruptions on global summer climate and East Asian Monsoon changes during the last millennium: Analysis of MPI-ESM simulations. *Journal of Climate, 27*(19), 7394-7409. doi:10.1175/jcli-d-13-00739.1

McKee, T. B., Doesken, N.J., & Kleist, J. (1993). *The relationship of drought frequency and duration to time scale.* Paper presented at the Proceedings of the Eighth Conference on Applied Climatology, American Meteorological Society, Anaheim, California.

PAGES 2k–PMIP3 group (2015). Continental-scale temperature variability in PMIP3 simulations and PAGES 2k regional temperature reconstructions over the past millennium. *Climate of the Past*, *11*(12), 1673-1699. doi:10.5194/cp-11-1673-2015

PAGES Hydro2k Consortium (2017). Comparing proxy and model estimates of hydroclimate variability and change over the Common Era. *Climate of the Past*, *13*(12), 1851-1900. doi:10.5194/cp-13-1851-2017

Palmer, W. C. (1965). Meteorological Drought. *Weather Bureau*, 45, 1-58.

Robock, A. (2000). Volcanic eruptions and climate. *Reviews of Geophysics, 38*(2), 191-219.

Robock, A. (2015): Volcanoes: Role in climate. In North, G. R., Pyle, J., & Zhang, F. Q. (Eds), *Encyclopedia of Atmospheric Sciences* (Vol. 2, pp. 105-111). San Diego, CA: Academic.

Schmidt, G. A., Jungclaus, J. H., Ammann, C. M., Bard, E., Braconnot, P., Crowley, T. J., et al. (2011). Climate forcing reconstructions for use in PMIP simulations of the last millennium (v1.0). *Geoscientific Model Development*, *4*(1), 33-45. doi:10.5194/gmd-4-33-2011

Schmidt, G. A., Kelley, M., Nazarenko, L., Ruedy, R., Russell, G. L., Aleinov, I., et al. (2014). Configuration and assessment of the GISS ModelE2 contributions to the CMIP5 archive. *Journal of Advances in Modeling Earth Systems*, *6*(1), 141-184. doi:10.1002/2013ms000265

Song, F., & Zhou, T. (2014). The climatology and interannual variability of East Asian Summer Monsoon in CMIP5 coupled models: Does air–sea coupling improve the simulations? *Journal of Climate, 27*(23), 8761-8777. doi:10.1175/jcli-d-14-00396.1

Stevenson, S., Fasullo, J. T., Otto-Bliesner, B. L., Tomas, R. A., & Gao, C. (2017). Role of eruption season in reconciling model and proxy responses to tropical volcanism. *Proceedings of* *the National Academy of Sciences of the United States of America, 114*(8), 1822-1826. doi:10.1073/pnas.1612505114

Stevenson, S., Otto-Bliesner, B., Fasullo, J., & Brady, E. (2016). “El Niño Like” Hydroclimate Responses to Last Millennium Volcanic Eruptions. *Journal of Climate, 29*(8), 2907-2921. doi:10.1175/jcli-d-15-0239.1

Sun, W. Y., Liu, J., Wang, B., Chen, D. L., Liu, F., Wang, Z. Y., et al. (2018). A “La Niña-like” state occurring in the second year after large tropical volcanic eruptions during the past 1500 years. *Climate Dynamics,* https://doi.org/10.1007/s00382-018-4163-x

Timmreck, C., Pohlmann, H., Illing, S., & Kadow, C. (2016). The impact of stratospheric volcanic aerosol on decadal-scale climate predictions. *Geophysical Research Letters, 43*(2), 834-842. doi:10.1002/2015gl067431

Trenberth, K. E., & Dai, A. (2007). Effects of Mount Pinatubo volcanic eruption on the hydrological cycle as an analog of geoengineering. *Geophysical Research Letters, 34*(15), L15702. doi:10.1029/2007gl030524

Wang, T., Guo, D., Gao, Y. Q., Wang, H. J., Zheng, F., Zhu, Y. L. et al. (2017). Modulation of ENSO evolution by strong tropical volcanic eruptions. *Climate Dynamics,* https://doi.org/10.1007/s00382-017-4021-2

Watanabe, M., Suzuki, T., O’ishi, R., Komuro, Y., Watanabe, S., Emori, S., et al. (2010). Improved Climate Simulation by MIROC5: Mean States, Variability, and Climate Sensitivity. *Journal of Climate, 23*(23), 6312-6335. doi:10.1175/2010jcli3679.1

Webb, R. W., Rosenzweig, C. E., & Levine, E. R. (2000). *Global soil texture and derived water-holding capacities.* Data Set available from http://www.daac.ornl.gov. Oak Ridge National Laboratory Distributed Active Archive Center. doi:10.3334/ORNLDAAC/548

Wegmann, M., Brönnimann, S., Bhend, J., Franke, J., Folini, D., Wild, M., & Luterbacher, J. (2014). Volcanic Influence on European Summer Precipitation through Monsoons: Possible Cause for “Years without Summer”. *Journal of Climate, 27*(10), 3683-3691. doi:10.1175/jcli-d-13-00524.1

Wu, D., Zhao, X., Liang, S., Zhou, T., Huang, K., Tang, B., & Zhao, W. (2015). Time-lag effects of global vegetation responses to climate change. *Global Chang Biology, 21*(9), 3520-3531. doi:10.1111/gcb.12945

Wu, T., Li, W., Ji, J., Xin, X., Li, L., Wang, Z., et al. (2013). Global carbon budgets simulated by the Beijing Climate Center Climate System Model for the last century. *Journal of Geophysical Research: Atmospheres, 118*(10), 4326-4347. doi:10.1002/jgrd.50320

Zambri, B., & Robock, A. (2016). Winter warming and summer monsoon reduction after volcanic eruptions in Coupled Model Intercomparison Project 5 (CMIP5) simulation. *Geophysical Research Letters,* 43, 10920-10928. doi:10.1002/2016GL070460

Zambri, B., Robock, A. N. L. A., & Slawinska, J. (2017). Northern Hemisphere winter warming and summer monsoon reduction after volcanic eruptions over the last millennium. *Journal of Geophysical Research-Atmospheres*, 122, 7971-7989. doi:10.1002/2017JD026728

Zhang, D., Blender, R., & Fraedrich, K. (2012). Volcanoes and ENSO in millennium simulations: global impacts and regional reconstructions in East Asia. *Theoretical and Applied Climatology, 111*(3-4), 437-454. doi:10.1007/s00704-012-0670-6

Zhou, T., Wu, B., Wen, X., Li, L., & Wang, B. (2008). A fast version of LASG/IAP climate system model and its 1000-year control integration. *Advances in Atmospheric Sciences, 25*(4), 655-672. doi:10.1007/s00376-008-0655-7

Zhuo, Z., Gao, C., & Pan, Y. (2014). Proxy evidence for China's monsoon precipitation response to volcanic aerosols over the past seven centuries. *Journal of Geophysical Research: Atmospheres, 119*(11), 6638-6652. doi:10.1002/2013JD021061

Figure 1.

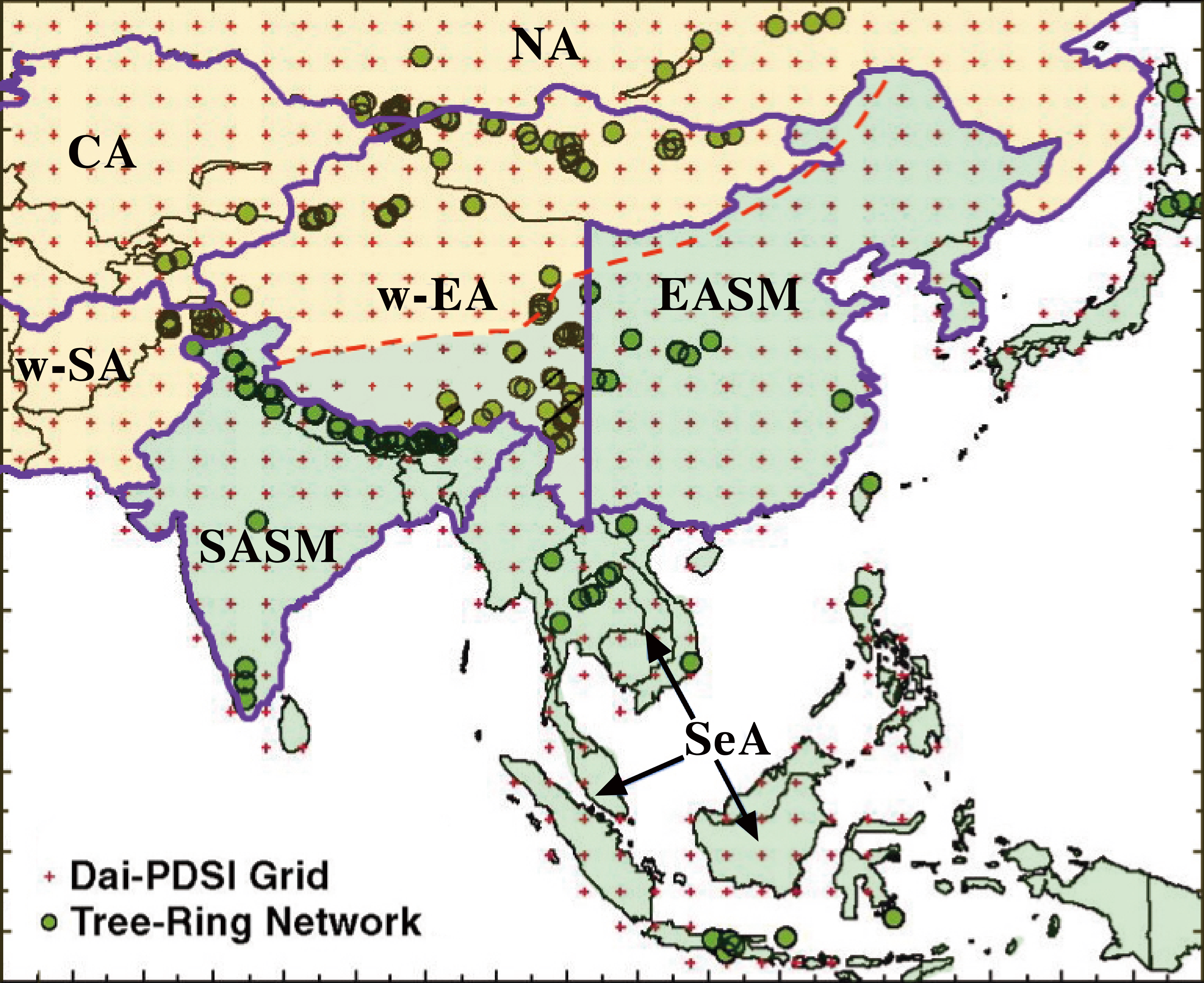
NA
CA
w-EA
EASM
w-SA
SASM
SeA
Dai-PDSI Grid
Tree-Ring Network

Figure 2.

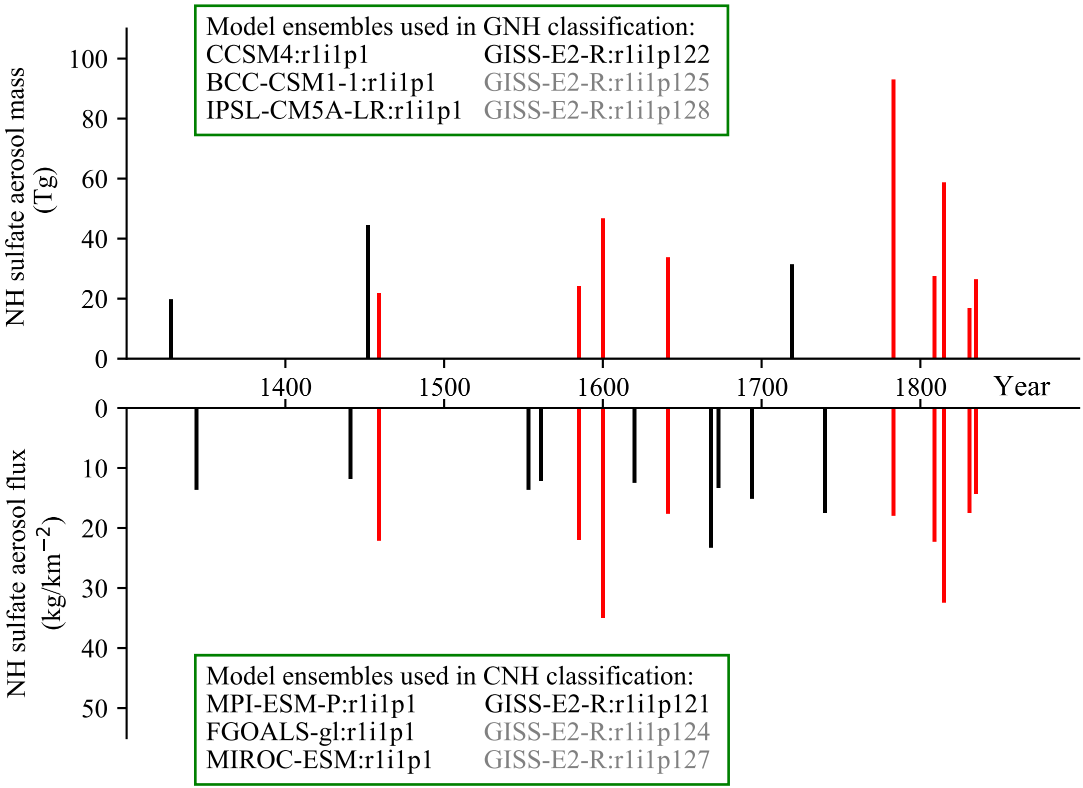
Model ensembles used in GNH classification:
CCSM4:r1i1p1
GISS-E2-R:r1i1p122
BCC-CSM1-1:r1i1p1
GISS-E2-R:r1i1p125
IPSL-CM5A-LR:r1i1p1
GISS-E2-R:r1i1p128
NH sulfate aerosol mass (Tg)
0
20
40
60
80
100
1400
1500
1600
1700
1800
Year
NH sulfate aerosol flux (kg/km^{-2})
0
10
20
30
40
50
Model ensembles used in CNH classification:
MPI-ESM-P:r1i1p1
GISS-E2-R:r1i1p121
FGOALS-gl:r1i1p1
GISS-E2-R:r1i1p124
MIROC-ESM:r1i1p1
GISS-E2-R:r1i1p127

Figure 3.

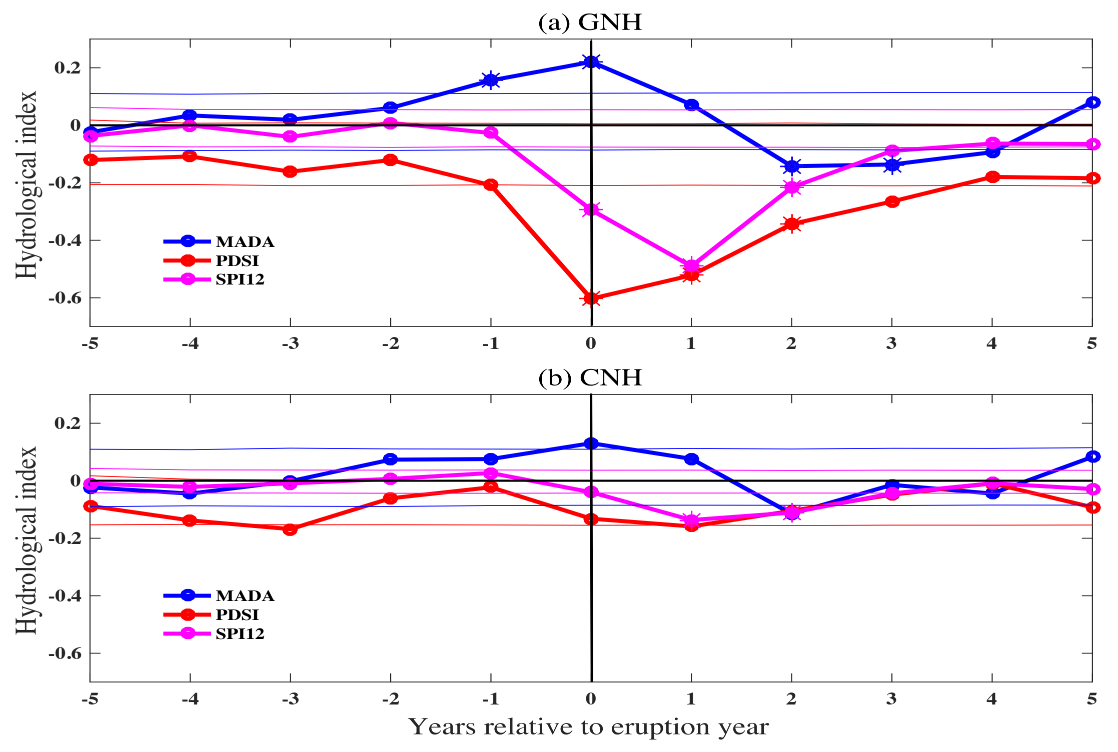

(a) GNH
Hydrological index
0.2
0
-0.2
-0.4
-0.6
MADA
PDSI
SPI12
-5
-4
-3
-2
-1
0
1
2
3
4
5
(b) CNH
Hydrological index
0.2
0
-0.2
-0.4
-0.6
MADA
PDSI
SPI12
-5
-4
-3
-2
-1
0
1
2
3
4
5
Years relative to eruption year

Figure 4.

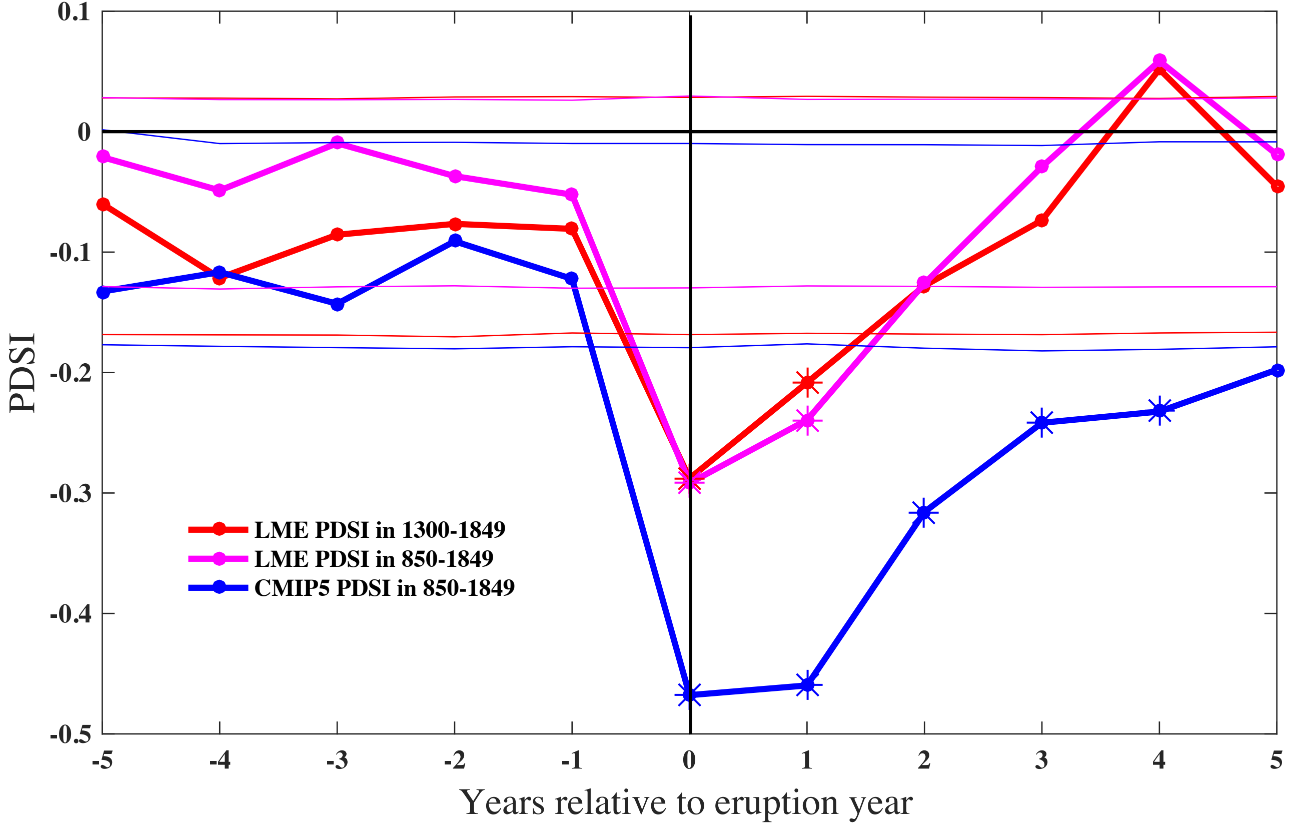
0.1
0
-0.1
-0.2
-0.3
-0.4
-0.5
PDSI
LME PDSI in 1300-1849
LME PDSI in 850-1849
CMIP5 PDSI in 850-1849
-5
-4
-3
-2
-1
0
1
2
3
4
5
Years relative to eruption year

Figure 5.

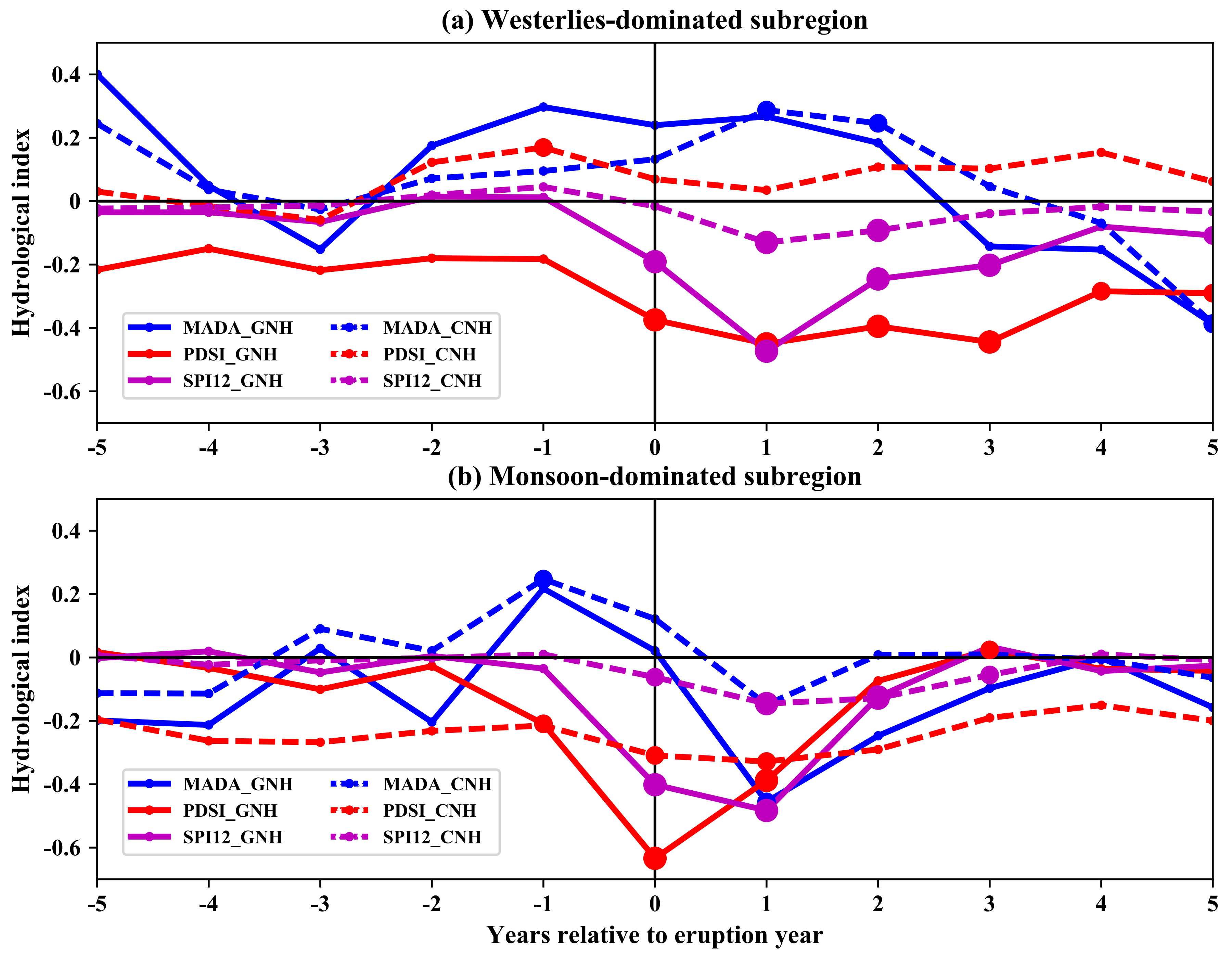

(a) Westerlies-dominated subregion
Hydrological index
0.4
0.2
0
-0.2
-0.4
-0.6
MADA_GNH
PDSI_GNH
SPI12_GNH
MADA_CNH
PDSI_CNH
SPI12_CNH
-5
-4
-3
-2
-1
0
1
2
3
4
5
(b) Monsoon-dominated subregion
Hydrological index
0.4
0.2
0
-0.2
-0.4
-0.6
MADA_GNH
PDSI_GNH
SPI12_GNH
MADA_CNH
PDSI_CNH
SPI12_CNH
-5
-4
-3
-2
-1
0
1
2
3
4
5
Years relative to eruption year

Figure 6.

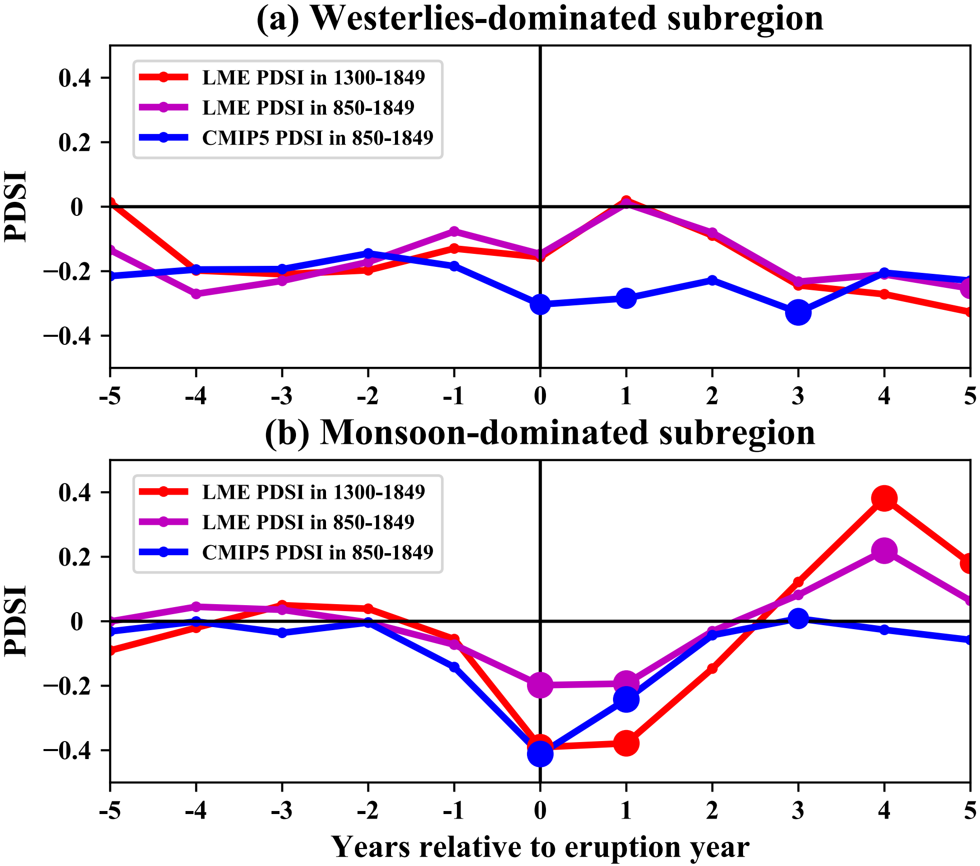
(a) Westerlies-dominated subregion
LME PDSI in 1300-1849
LME PDSI in 850-1849
CMIP5 PDSI in 850-1849
PDSI
0.4
0.2
0
−0.2
−0.4
-5
-4
-3
-2
-1
0
1
2
3
4
5
(b) Monsoon-dominated subregion
LME PDSI in 1300-1849
LME PDSI in 850-1849
CMIP5 PDSI in 850-1849
PDSI
Years relative to eruption year

Figure 7.

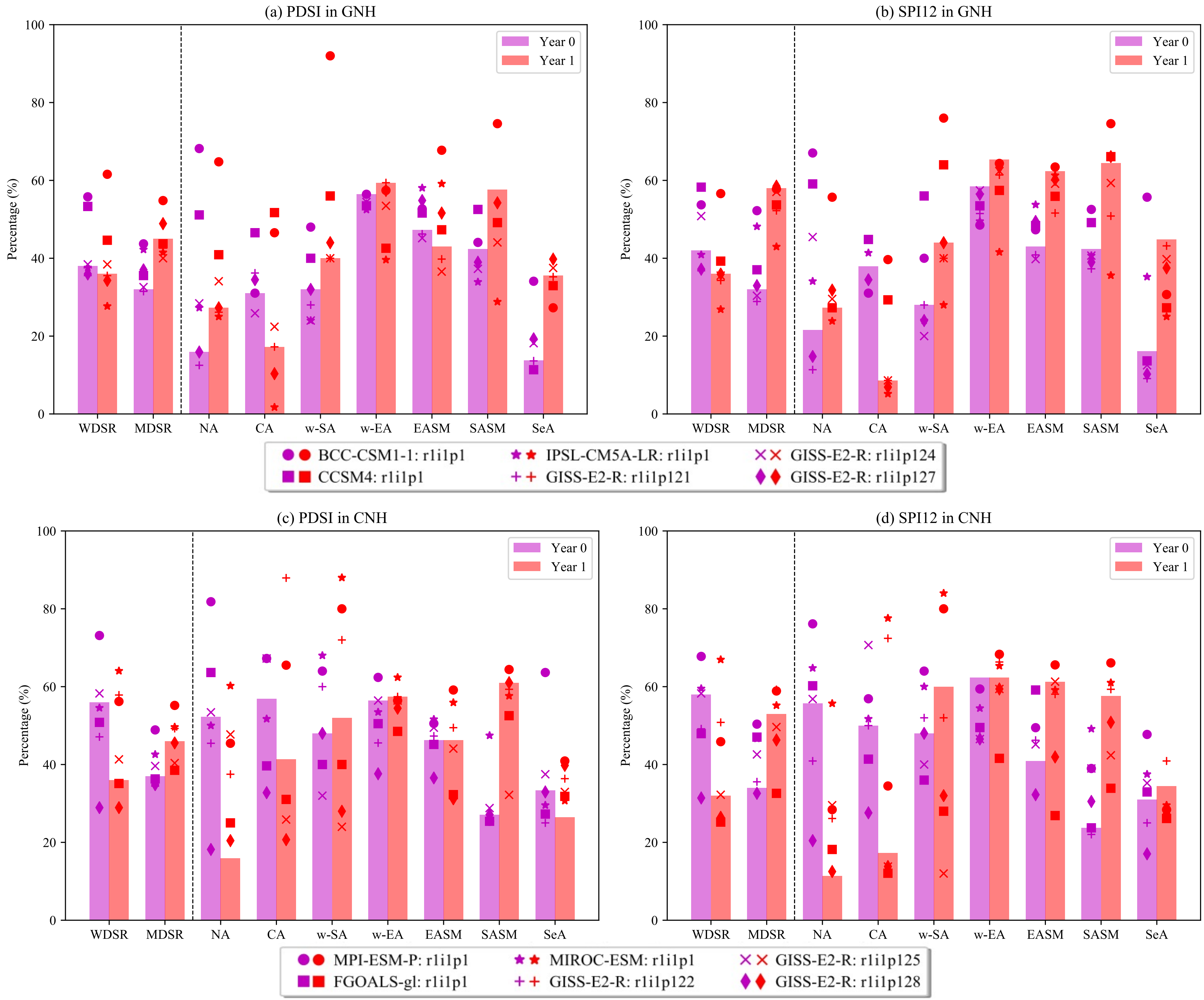

(a) PDSI in GNH
(b) SPI12 in GNH
(c) PDSI in CNH
(d) SPI12 in CNH
Percentage (%)
Year 0
Year 1
WDSR
MDSR
NA
CA
w-SA
w-EA
EASM
SASM
SeA
BCC-CSM1-1: r1i1p1
CCSM4: r1i1p1
IPSL-CM5A-LR: r1i1p1
GISS-E2-R: r1i1p121
GISS-E2-R: r1i1p124
GISS-E2-R: r1i1p127
MPI-ESM-P: r1i1p1
FGOALS-gl: r1i1p1
MIROC-ESM: r1i1p1
GISS-E2-R: r1i1p122
GISS-E2-R: r1i1p125
GISS-E2-R: r1i1p128

Figure 8.

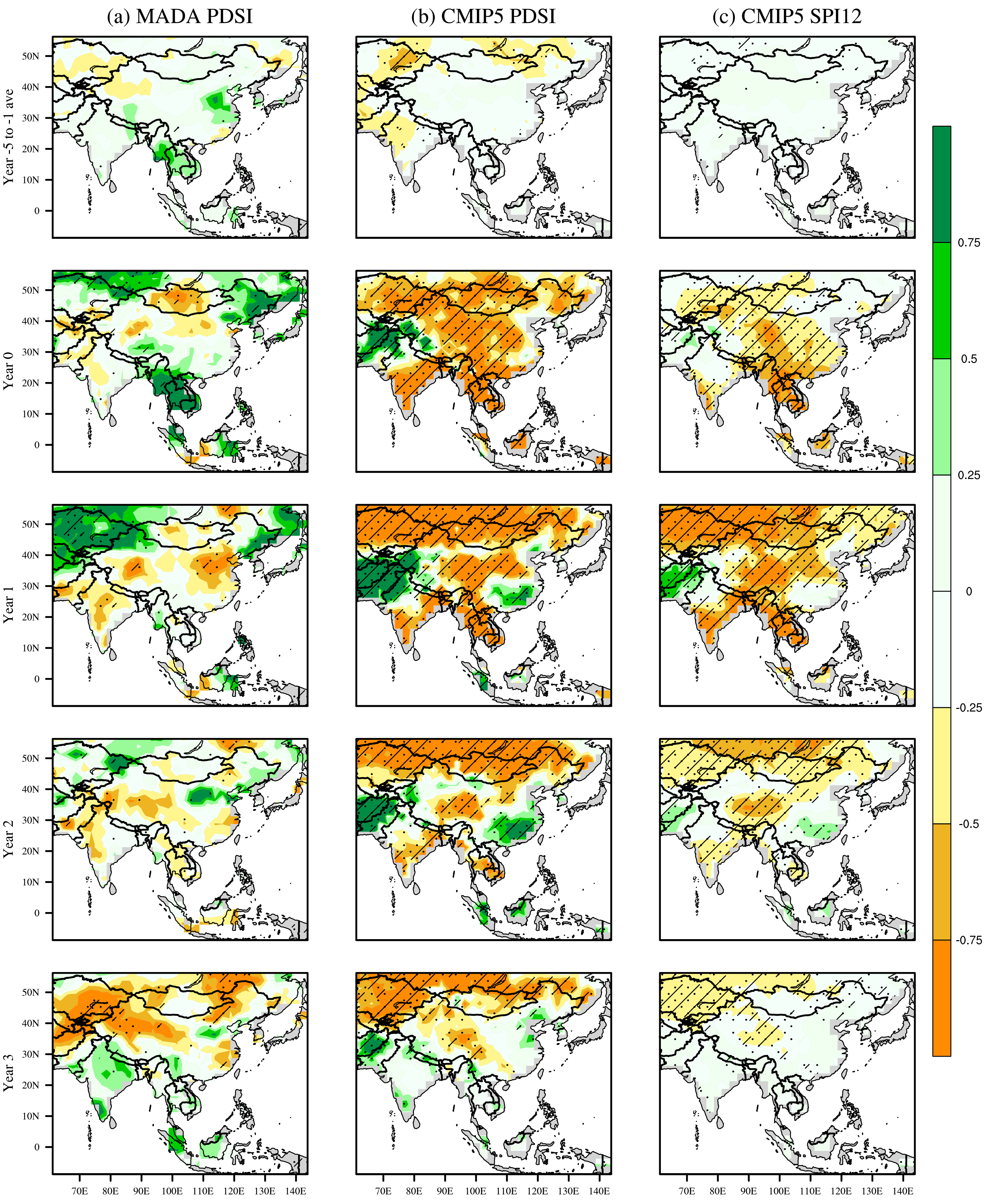

(a) MADA PDSI
(b) CMIP5 PDSI
(c) CMIP5 SPI12
Year -5 to -1 ave
Year 0
Year 1
Year 2
Year 3
50N
40N
30N
20N
10N
0
70E
80E
90E
100E
110E
120E
130E
140E
0.75
0.5
0.25
0
-0.25
-0.5
-0.75

Figure 9.

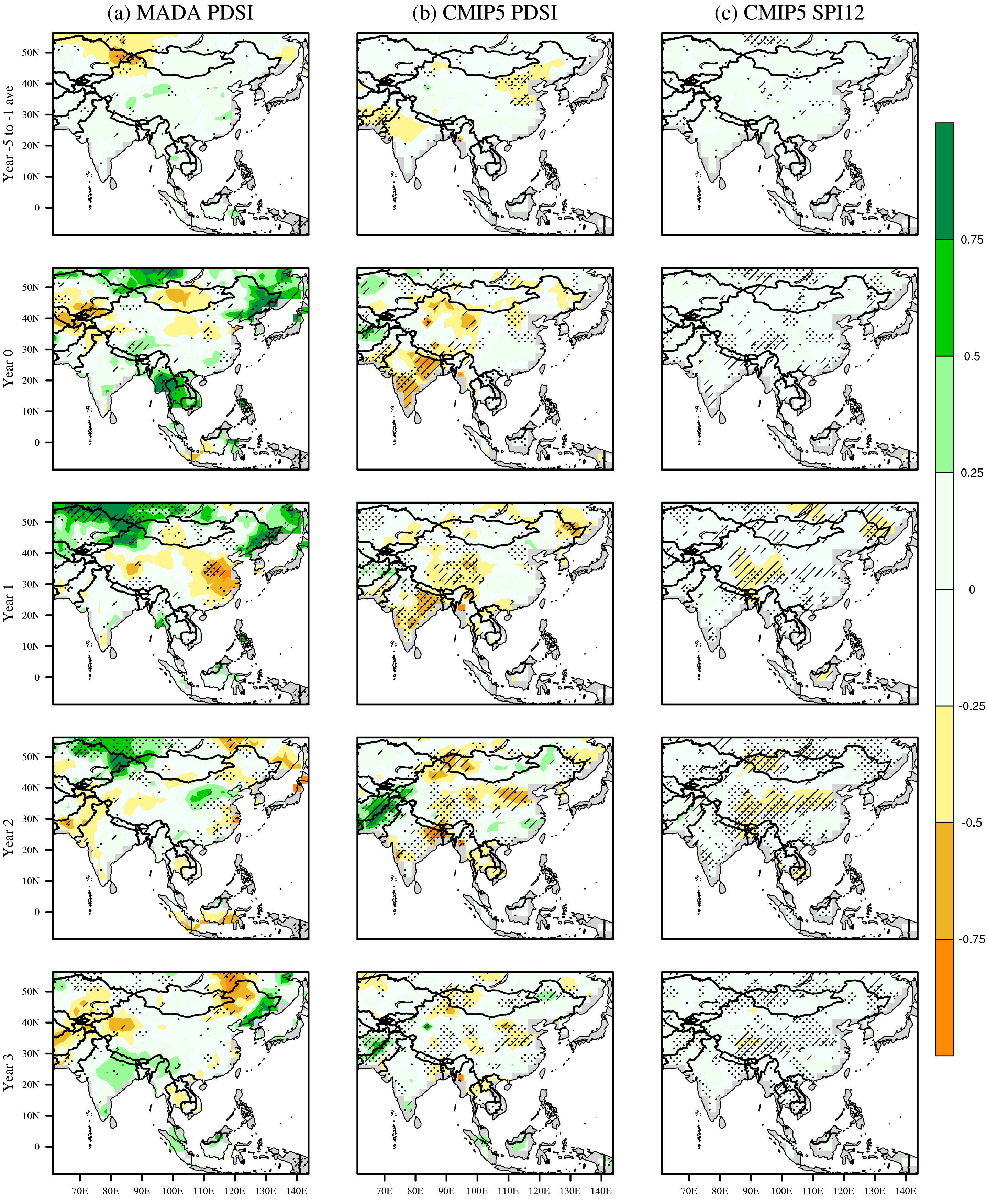

(a) MADA PDSI
(b) CMIP5 PDSI
(c) CMIP5 SPI12
Year -5 to -1 ave
Year 0
Year 1
Year 2
Year 3
50N
40N
30N
20N
10N
0
70E
80E
90E
100E
110E
120E
130E
140E
0.75
0.5
0.25
0
-0.25
-0.5
-0.75

Figure 10.

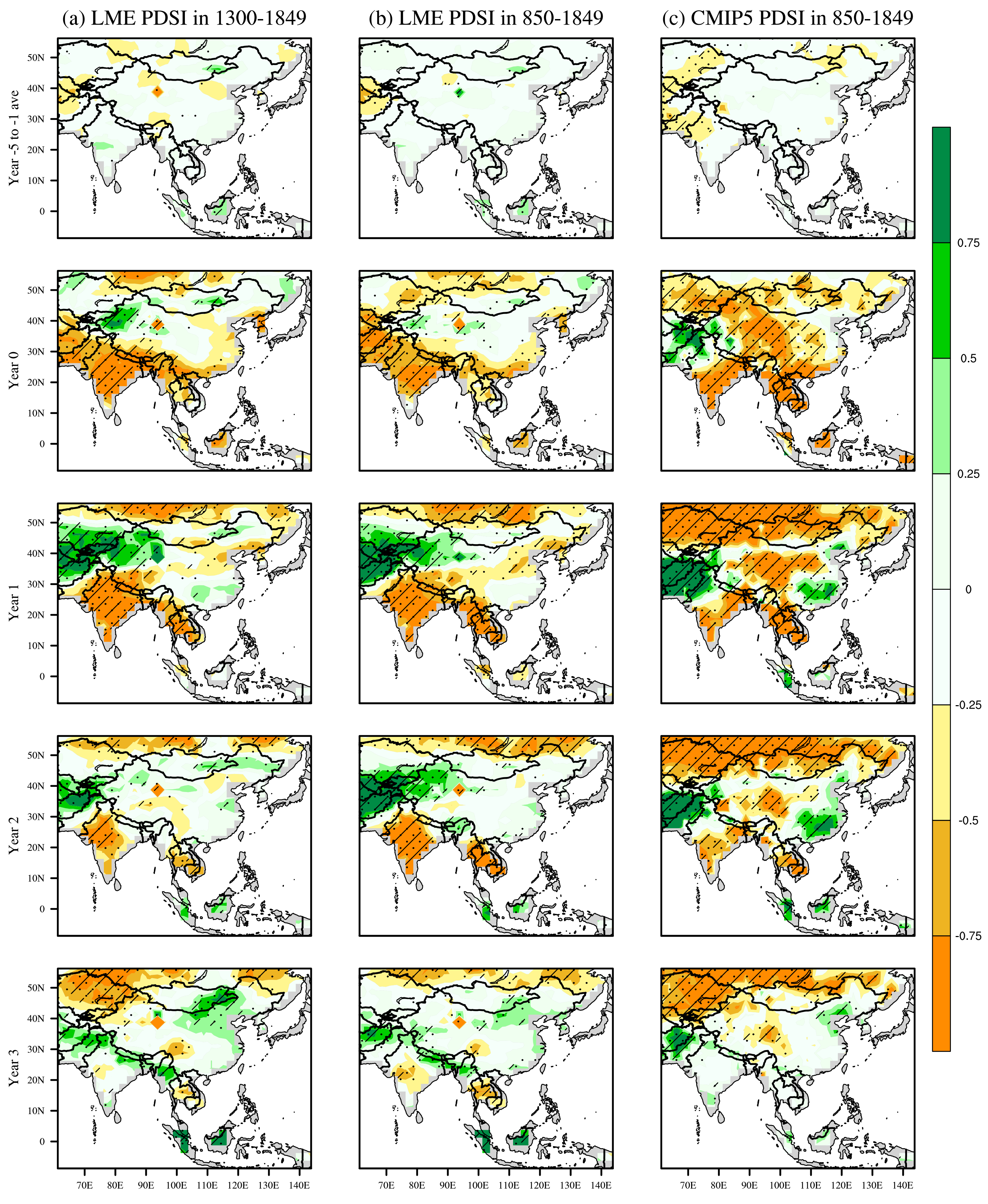

(a) LME PDSI in 1300-1849
(b) LME PDSI in 850-1849
(c) CMIP5 PDSI in 850-1849
Year -5 to -1 ave
Year 0
Year 1
Year 2
Year 3
50N
40N
30N
20N
10N
0
70E
80E
90E
100E
110E
120E
130E
140E
0.75
0.5
0.25
0
-0.25
-0.5
-0.75

Figure 11.

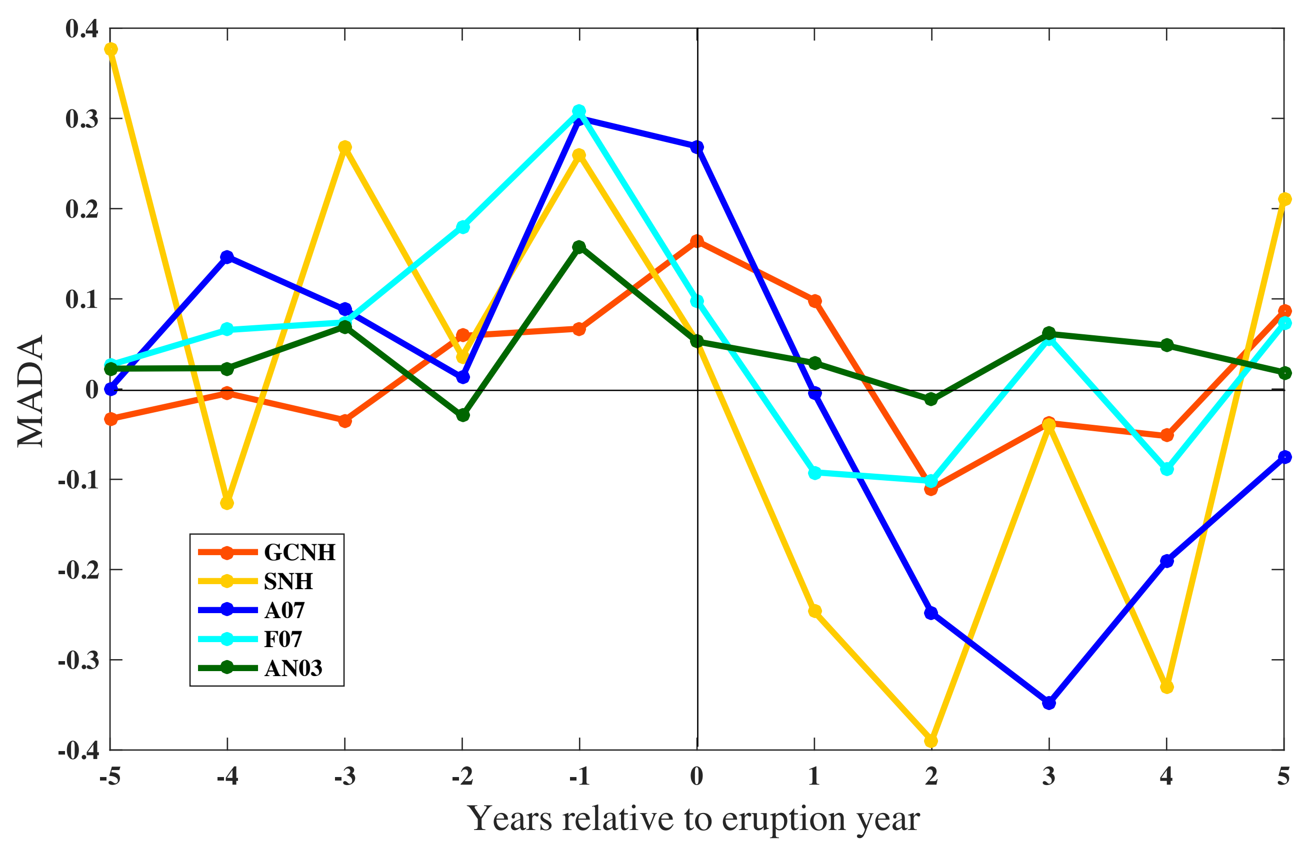

0.4
0.3
0.2
0.1
0
-0.1
-0.2
-0.3
-0.4
MADA
-5
-4
-3
-2
-1
0
1
2
3
4
5
Years relative to eruption year
GCNH
SNH
A07
F07
AN03

Journal of Geophysical Research: Atmospheres

Supporting Information for

Comparison of Proxy and Multi-Model Ensemble Mean on Volcanic Aerosols' Hydrological Effects in Asian Monsoon and Westerlies-dominated Subregions

Z. Zhuo[1], C.C. Gao[2], I. Kirchner[1] and U. Cubasch[1]

[1]Institute of meteorology, Freie Universität Berlin, Berlin, Germany. [2]Department of Environmental Science, Zhejiang University, Hangzhou, China.

Contents of this file

Tables S1 to S3

Introduction

Table S1 lists the information about CMIP5 model ensembles used.

Table S2 lists the volcanic eruption years and northern hemisphere volcanic aerosol injections in the two classifications.

Table s3 lists the tested classifications of volcanic events and their dated years for proxy reconstruction data

Table S1
CMIP5 model ensembles used.

Model	Ensemble	Resolution (°) (lat **x** lon)	Vertical levels	Volcanic forcing	References
CCSM4	r1i1p1	0.94 x 1.25	26	GRA	Gent et al., 2011
BCC-CSM1-1	r1i1p1	2.8 x 2.8	26	GRA	Wu et al., 2013
IPSL-CM5A-LR	r1i1p1	1.9x3.75	39	GRA	*Dufresne et al.,* 2013
GISS-E2-R	r1i1p121 r1i1p125 r1i1p128	2x2.5	40	GRA	*Schmidt et al.,* 2014
MPI-ESM-P	r1i1p1	1.865x1.875	47	CEA	*Giorgetta et al.,* 2013
FGOALS-gl	r1i1p1	5x4	26	CEA	Zhou et al., 2008
MIROC-ESM	r1i1p1	2.8x2.8125	80	CEA	*Watanabe et al.,* 2011
GISS-E2-R	r1i1p122 r1i1p124 r1i1p127	2x2.5	40	CEA	*Schmidt et al.,* 2014

Table S2

List of eruption year and northern hemisphere aerosol injection in two volcanic classifications.

Eruption Year (CE)	GNH Sulfate Aerosol Mass[a] (Tg)	CNH Sulfate Aerosol Flux[b] ($kg*km^{-2}$)
1328	19.7	
1344		13.6
1441		11.8
1452	44.6	
1459	21.9	22.1
1553		13.6
1561		12.2
1585	24.2	22.0
1600	46.1	35.0
1620		12.4
1641	33.8	17.6
1668		23.3
1673		13.3
1694		15.1
1719	31.5	
1740		17.5
1783	93.0	17.9
1809	27.6	22.2
1815	58.7	32.5
1831	17.0	17.5
1835	26.4	14.3

Note. [a]Aerosol mass is based on GRA volcanic forcing from Gao et al. (2008). [b]Aerosol flux is based on CEA volcanic forcing from Crowley et al. (2013). Years in bold are the volcanic events included in both classifications.

Table s3

Tested classifications of volcanic events and their dated years for proxy reconstruction data.

Classification	Reference	Event Year (CE)	Num.
GCNH [a]	Gao et al., 2008; Crowley et al., 2008	1328, 1344, 1441, 1452, 1459, 1553, 1561, 1585, 1600, 1620, 1641, 1668, 1673, 1694, 1719, 1740, 1783, 1809, 1815, 1831, 1835	21
SNH [b]	Sigl et al., 2015	1345, 1458, 1601, 1641, 1695, 1783, 1809, 1815, 1836	9
A07	Ammann et al., 2007	1452, 1600, 1641, 1809, 1815	5
F07	Fischer et al., 2007	1586, 1596, 1600, 1641, 1673, 1809, 1815, 1823, 1831, 1835	10
AN03	Ammann and Naveau, 2003	1443, 1452, 1459, 1463, 1490, 1504, 1512, 1522, 1554, 1568, 1571, 1586, 1595, 1600, 1605, 1619, 1622, 1641, 1660, 1665, 1674, 1680, 1693, 1712, 1721, 1728, 1737, 1744, 1749, 1752, 1760, 1774, 1789, 1794, 1808, 1813, 1823, 1831, 1835	39

Note. [a]Combination of both volcanic events in the GNH and CNH classifications. [b]Volcanic events have larger global forcing and more sulfate in Greenland than that of Pinatubo eruption in 1991, selection is based on Sigl et al. (2015) reconstruction. The other three classifications are following that in Anchukaitis et al. (2010), which are classifications used by the reference papers. Here, we remove the latter year if two events happened in less than three years.